

Tumor-intrinsic *RGS1* potentiates checkpoint blockade response via ATF3-IFNGR1 axis

Baojun Wang^{a,b*}, Bo Jiang^{b*}, Lin Du^{c*}, Wenyuan Chen^a, Qing Zhang^b, Wei Chen^b, Meng Ding^b, Wenmin Cao^b, Jie Gao^b, Yongming Deng^b, Yao Fu^d, Yan Li^e, Yonglong Xiao^e, Wenli Diao^b, and Hongqian Guo^{a,b}

^aDepartment of Urology, Nanjing Drum Tower Hospital Clinical College of Nanjing University of Chinese Medicine, Nanjing, Jiangsu, China;

^bDepartment of Urology, Nanjing Drum Tower Hospital, The Affiliated Hospital of Nanjing University Medical School, Nanjing, Jiangsu, China;

^cDepartment of Urology, Nanjing Drum Tower Hospital, The Affiliated Hospital of Southeast University Medical School, Nanjing, Jiangsu, China;

^dDepartment of Pathology, Nanjing Drum Tower Hospital, The Affiliated Hospital of Nanjing University Medical School, Nanjing, Jiangsu, China;

^eDepartment of Respiratory and Critical Care Medicine, The Affiliated Drum Tower Hospital of Nanjing University Medical School, Nanjing, China

ABSTRACT

Background: Non-responsiveness is a major barrier in current cancer immune checkpoint blockade therapies, and the mechanism has not been elucidated yet. Therefore, it is necessary to discover the mechanism and biomarkers of tumor immunotherapeutic resistance.

Methods: Bioinformatics analysis was performed based on CD8⁺ T cell infiltration in multiple tumor databases to screen out genes related to anti-tumor immunity. Associations between Regulator of G-protein signaling 1 (*RGS1*) and IFN γ -STAT1 signaling, and MHC I antigen presentation pathway were examined by RT-qPCR, western blotting, and flow cytometry. The modulatory mechanisms of *RGS1* were investigated via CHIP-qPCR and dual-luciferase assay. The clinical and therapeutic implications of *RGS1* were comprehensively investigated using tumor cell lines, mouse models, and clinical samples receiving immunotherapy.

Results: *RGS1* was identified as the highest gene positively correlated with immunogenicity among *RGS* family. Inhibition of *RGS1* in neoplastic cells dampened anti-tumor immune response and elicited resistance to immunotherapy in both renal and lung murine subcutaneous tumors. Mechanistically, *RGS1* enhanced the binding of activating transcription factor 3 (ATF3) to the promoter of interferon gamma receptor 1 (IFNGR1), activated STAT1 and the subsequent expression of IFN γ -inducible genes, especially CXCL9 and MHC class I (MHC I), thereby influenced CD8⁺ T cell infiltration and antigen presentation and processing. Clinically, lower expression level of *RGS1* was associated with resistance of PD1 inhibition therapy and shortened progression-free survival among 21 NSCLC patients receiving immunotherapy.

Conclusions: Together, these findings uncover a novel mechanism that elicits immunotherapy resistance and highlight the function of tumor-intrinsic *RGS1*, which brings new insights for future strategies to sensitize anti-PD1 immunotherapy.

ARTICLE HISTORY

Received 31 May 2023

Revised 12 October 2023

Accepted 1 November 2023

KEYWORDS

IFN γ signaling;
immunotherapy; NSCLC;
RCC; *RGS1*

Introduction




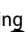

Immune checkpoint blockade (ICB) therapy that unleashes CD8⁺ T cell-mediated anti-tumor immunity has shown unprecedented success in various “hot” tumors.^{1–3} However, even fighting against “hot” tumors as clear-cell renal cell carcinoma (ccRCC) and non-small cell lung carcinoma (NSCLC), more than 40% of treated individuals were refractory to anti-programmed cell death protein 1 (PD1)/PD-L1 therapy. Therefore, it is in urgent need to identify accurate predictive biomarkers and understand the mechanism eliciting immunotherapy resistance.

Tumors exploit various mechanisms to manipulate the integrity of interferon γ (IFN γ) signaling and thus drive immune evasion and blunt immunotherapy efficacy.^{4–12} In addition, MHC class I (MHC I) mutations,¹⁰ diminished transcription,¹³


and degradation¹⁴ also contribute to tumor immune evasion and checkpoint therapy resistance. However, there has been limited studies on lung and renal cancers in this regard.

Regulators of G-protein signaling (RGS) are a family of related proteins that negatively regulate G-protein coupled receptor (GPCR) signaling.¹⁵ As a member of RGS family, *RGS1* in T cells has been recently associated with T cell recruitment.^{16,17} However, the role of tumor-intrinsic *RGS1* in anti-tumor immunity and response to immunotherapy has not been elucidated.

Here, by bioinformatics analysis and preclinical mouse models, we demonstrate that *RGS1* in neoplastic cells benefits checkpoint therapy in renal and lung cancers by enhancing tumor immunogenicity and anti-tumor immune response. Our research

CONTACT Hongqian Guo  dr.ghq@nju.edu.cn; Wenli Diao  diaowl@126.com  Department of Urology, Nanjing Drum Tower Hospital, Clinical College of Nanjing University of Chinese Medicine, 321 Zhongshan Road, Nanjing, Jiangsu Province 210008, China; Yonglong Xiao  yonglong11a@163.com  Department of Respiratory and Critical Care Medicine, The Affiliated Drum Tower Hospital of Nanjing University Medical School, 321 Zhongshan Road, Nanjing, Jiangsu Province 210008, China

*These authors contributed equally to this work.

 Supplemental data for this article can be accessed online at <https://doi.org/10.1080/2162402X.2023.2279800>

© 2023 The Author(s). Published with license by Taylor & Francis Group, LLC.

This is an Open Access article distributed under the terms of the Creative Commons Attribution-NonCommercial License (<http://creativecommons.org/licenses/by-nc/4.0/>), which permits unrestricted non-commercial use, distribution, and reproduction in any medium, provided the original work is properly cited. The terms on which this article has been published allow the posting of the Accepted Manuscript in a repository by the author(s) or with their consent.

elucidates the pivotal role of RGS1 in tumor immunotherapeutic response from a novel angle, and may open new directions for combination therapy design to reverse immunotherapeutic resistance.

Materials and methods

Cell culture

All cells were routinely cultured at 37°C in a humidified incubator with 5% CO₂. 293T (human embryonic kidney cells), 786O (human RCC line), and A549 (human NSCLC line) were obtained from the Cell Bank of the Chinese Academy of Science (Shanghai, China). Renca (murine RCC line) and LLC (Lewis lung cancer line) were purchased from the American Type Culture Collection (Rockville, MD, USA). Except as otherwise noted, all the cell lines were cultured in the recommended medium of ATCC (Sigma-Aldrich) supplemented with 10% fetal bovine serum (FBS, Thermo Fisher Scientific) and 1% penicillin/streptomycin (10,000 U/mL, Thermo Fisher Scientific).

Plasmid, lentivirus construction, and transfection

For stable RGS1 knockdown, human and mouse small hairpin RNA (shRNA) lentiviral vectors targeting RGS1 (shRGS1 and shRgs1, respectively) were purchased from GenePharma (Shanghai, China). The target sequences were shown as follows: shRGS1-1: GTCCAAGGATGTACTTTCT; shRGS1-2: CCAAGAAGATTAAAGCACCAA; shRgs1-1: GCATTTGTGCATTCAGATGCT; shRgs1-2: GAGATCGATGATCCACATCT. For the transient reporter analysis, the promoter of human *IFNGR1* was inserted into the pmirGLO reporter plasmid, and the two sequences that may interact with ATF3 were mutated and inserted into an equivalent pmirGLO reporter plasmid; both plasmids were synthesized by Tsingke Biotechnology, and the specific mutant sequences of the hypothetical binding sites are listed in Figure 4s.

Luciferase assay

To determine the binding region in *IFNGR1* promoter for ATF3, we transfected 293T cells with pmirGLO-*IFNGR1* control, pmirGLO-*IFNGR1* mut, pcDNA3.1-Flag control and pcDNA3.1-Flag-ATF3. After 48 hours, relative luciferase units were measured with Dual Luciferase Reporter Gene Assay Kit (Beyotime) according to the manufacturer's instructions. The units of relative luciferase are the ratio of firefly luciferase signal to Renilla signal.

Animal experiments

The animal experiments were approved by the Institutional Animal Care and Use Committee of Nanjing Drum Tower Hospital. Eight-week-old male BALB/c mice and C57BL/6 mice were purchased from the Animal Core Facility of Nanjing Medical University. ShRgs1 or RGS1-overexpressing Renca/LLC cells, and the corresponding CTRL or Vector cells were harvested for

allograft tumor models. For murine renal tumor model, 2×10^5 Renca cells were injected subcutaneously into Balb/c mice; for murine lung tumor model, 2×10^6 LLC cells were injected subcutaneously into C57BL/6 mice, in a volume of 100 μ L medium, respectively. PD1 antibody (BioXcell, clone RMP1-14) or IgG control (100 μ g/mouse) were administered via *intraperitoneal injection (I.P)* for 4 times every 3 d. The tumors were measured daily with calipers, and tumor volumes = length \times width²/2. Once the tumor reached 1000 mm³, ulceration occurred, or the animal showed signs of distress, the mice were sacrificed. Tumors were obtained and immobilized with 10% buffered formalin phosphate for immunohistochemistry (IHC) and immunofluorescence staining.

In vitro T cell killing assay

Transgenic OT-I mice were generously donated by Professor Tang Hua from Shandong First Medical University, China. CD8⁺ T cells were isolated from spleens of transgenic OT-I mice using EasySepTM mouse CD8⁺ T Cell Isolation Kit (Stemcell) according to the instructions. Briefly, the spleens of OT-I mice were sheared and passed through a 70- μ m cell strainer. After red blood cells were depleted, the remaining cells were resuspended in sorting buffer (PBS containing 2% FBS and 1 mM EDTA) and incubated with rat serum and isolated cocktail for 10 minutes. Then the magnetic beads were added and incubated for 5 minutes, and the tube was put in a magnetic rack. Another 5 minutes later, the supernatant poured out were mostly CD8⁺ T cells. After washed with PBS, the cells were resuspended in RPMI-1640 medium supplemented with anti-mouse CD28 antibody (1 μ g/mL) and 10% FBS, and seeded into a 96-well plate pre-coated with anti-mouse CD3 antibody (1 μ g/mL). After 48 hours of stimulation, activated CD8⁺ T cells were seeded into a new plate with fresh medium containing mouse recombinant IL-2 (5 μ g/ml) and incubated for another 2 d. Nc-LLC-OVA and shRgs1-LLC-OVA cells (1×10^5) were seeded overnight and pretreated with OVA peptides for 2 hours as previous reported.^{10,18} CD8⁺ T cells were then added into the culture system in different proportions (E:T= 10:1, 5:1, 2:1, 0:1). After 24-hour co-culturation, the level of IFN γ in the supernatant was determined by enzyme-linked immunosorbent assay (ELISA) and the remaining tumor cells were analyzed by flow cytometry.

Western blotting

For western blotting, protein extracts were separated by 10% or 12% sodium dodecyl sulfate polyacrylamide gel electrophoresis (SDS-PAGE) and transferred to polyvinylidene fluoride (PVDF) membranes. After blocking with 5% nonfat milk in PBS containing 0.1% Tween-20, the membrane was incubated with appropriate primary antibodies overnight at 4°C, and then incubated with horseradish peroxidase-conjugated secondary antibodies for another 1 hour at room temperature. The membranes were then incubated with electrochemiluminescence substrate (ECL, Vazyme) and the protein levels were visualized using

chemiluminescence imager (Clinx Science Instruments Co., Shanghai, China). Antibodies and reagents are shown in Table S1

Clinical tissue samples

Paraffin sections of NSCLC patients were obtained from Nanjing Drum Tower Hospital. Patients were divided into 10 responders (complete or partial response or stable disease) and 11 non-responders (progressive disease), following standard Response Evaluation Criteria In Solid Tumors (RECIST v1.1) guidelines. Human ccRCC tissue microarrays were obtained from Nanjing Drum Tower Hospital. The study protocol was under the approval of the Institutional Review Board of Nanjing Drum Tower Hospital (approval 2017-147-01). The collection of all tissue samples was in compliance with informed consent policy.

Immunohistochemistry and immunofluorescence staining

4 mm paraffin sections of patient or mouse samples were baked at 75°C for 120 min, dewaxed in xylene three times for 10 min, and rehydrated in 100%, 90%, 80%, and 70% ethanol solutions for 2 min, respectively. The slides were blocked in 5% BSA for 1 h at room temperature and incubated with primary antibody overnight at 4°C. For immunohistochemistry (IHC), the slides were incubated with secondary antibodies (Vector Laboratories, Burlingame, CA, USA) for 1 hour at room temperature, and the target proteins were detected by DAB detection kit (ZsBio, Beijing, China). Each slide was further scanned and analyzed using NanoZoomer S60 (Hamamatsu Photonics) and Image J software. Multiple random fields on the slice were chosen for analysis, with staining intensity scored as 0 (negative), 1 (low), 2 (moderate), 3 (high) and 4 (extremely high). The percentage of staining area was analyzed with a range from 0 to 100%. The staining score was obtained by multiplying the intensity score by staining range (%). For immunofluorescence staining, the slides were further incubated with fluorescence-labeled secondary antibodies for 1 hour at room temperature, and the nuclei were stained with DAPI (Beyotime) for 10 minutes, kept in dark place. Samples were observed using a fluorescence microscope (Leica DMi8, Leica Biosystems Inc.). Analysis and quantification of the images were performed by 3D HISTECH quant center 2.1 software. Staining intensity was scored from 0 to 3. Staining percentage of each staining area were analyzed with a range from 0 to 100%. The result of staining intensity multiplied by the percentage of positive cells yields a Histo score, which is ranged from 0 to 300%. To divide RGS expression, the Histo score $\leq 150\%$ was considered as low expression, and $>150\%$ as high expression as previously described¹⁹.

Flow cytometry analysis

For detection of cell surface MHCI and IFNGR1, cells were blocked with 1% BSA for 30 minutes at 4°C, followed by incubation with fluorescent antibodies or isotype antibodies at 4°C for another 30 minutes. Data acquisition was performed with a NovoCyte device (Agilent Technologies Inc., Santa Clara, CA, USA). All analysis was performed using FlowJo version 10 software.

Chromatin immunoprecipitation

We performed chromatin immunoprecipitation (ChIP) assays according to the protocol of SimpleChIP Plus Ultrasonic Chromatin IP Kit (CST, 9005). Briefly, cells were incubated with 1% formaldehyde for 10 min at room temperature to allow proteins to cross-link with DNA, and the nuclei were degraded with micrococcal nuclease and ultrasonication. Cross-linked and digested chromatin was immunoprecipitated with indicated antibodies. Immunoprecipitated chromatin was incubated with 5 M NaCl and Proteinase K at 65°C to reverse cross-links, followed by DNA purification. The DNA was quantified by RT-qPCR with specific primers listed in Table S2.

ELISA

Cells (1×10^6) with complete growth medium were seeded in 6-well plates and cultured overnight. On the following day, cells were washed with PBS and treated with 5 ng/ml IFN γ for 24 hours. The concentrations of mouse CXCL9/MIG, human cAMP level and the activity of PKA in the supernatants were analyzed using CXCL9 ELISA kit (R&D Systems, MCX900), cAMP ELISA Kit (Elabscience, E-EL-0056c) and PKA Colorimetric Activity Kit (Thermo Fisher scientific, EIAPKA) respectively, according to the manufacturer's protocols. Microplate reader was set to 450 nm to determine the optical density.

Real-time PCR analysis

According to the manufacturer's instructions, total RNA was extracted with TRIzol reagent (Invitrogen). For quantitative RT-PCR (RT-qPCR), cDNA, SYBR Premix Ex Taq™ (Takara) and specific primers were in use. The sequences of the primers are listed in Table S3. All primers were synthesized by Generay Biotech (Shanghai) Co., Ltd. The expression of relevant mRNAs was normalized with β -actin. Comparative CT method was used to calculate the fold change of gene expression.

Bioinformatics analysis

ccRCC (KIRC, 523 samples), NSCLC (LUAD, 483 samples and LUSC, 486 samples) and melanoma (SKCM, 461 samples) data were downloaded from The Cancer Genome Atlas (TCGA, R-package) and log2 transformed. We used normalized expression of genes to define the signatures: CD8⁺ T-cell infiltration (CD8A, CD8B, PRF1 and GZMB) according to the previous literature.²⁰ Then, we defined top 10% as "hot" tumors and bottom 10% as "cold" tumors in the CD8⁺ T-cell infiltration cohort, and performed differential expression analysis in "hot" tumors versus "cold" tumors, respectively. Statistical analysis was performed using R version 3.5.2 (packages limma, dplyr, ggrepel and ggplot 2). Further, we performed Gene Set Enrichment Analysis (GSEA) analysis according to the manufacturer's protocol.

Statistical analysis

All data were analyzed with Graphpad Prism V9. Data from at least three independent experiments are presented as the mean \pm SD. Two-sample comparisons were using student t-test. Tumor growth data were analyzed via two-way ANOVA. Survival curves were analyzed by log-rank test. * $p < .05$, ** $p < .01$, *** $p < .001$ were considered statistically significant.

Results

Tumor-intrinsic RGS1 is positively associated with tumor immunogenicity

To identify potential immunoregulatory factors, we performed differential gene analysis between “hot” and “cold” tumors. The design and implementation of this investigation are shown in Figure 1a. We first analyzed ccRCC (KIRC, 523

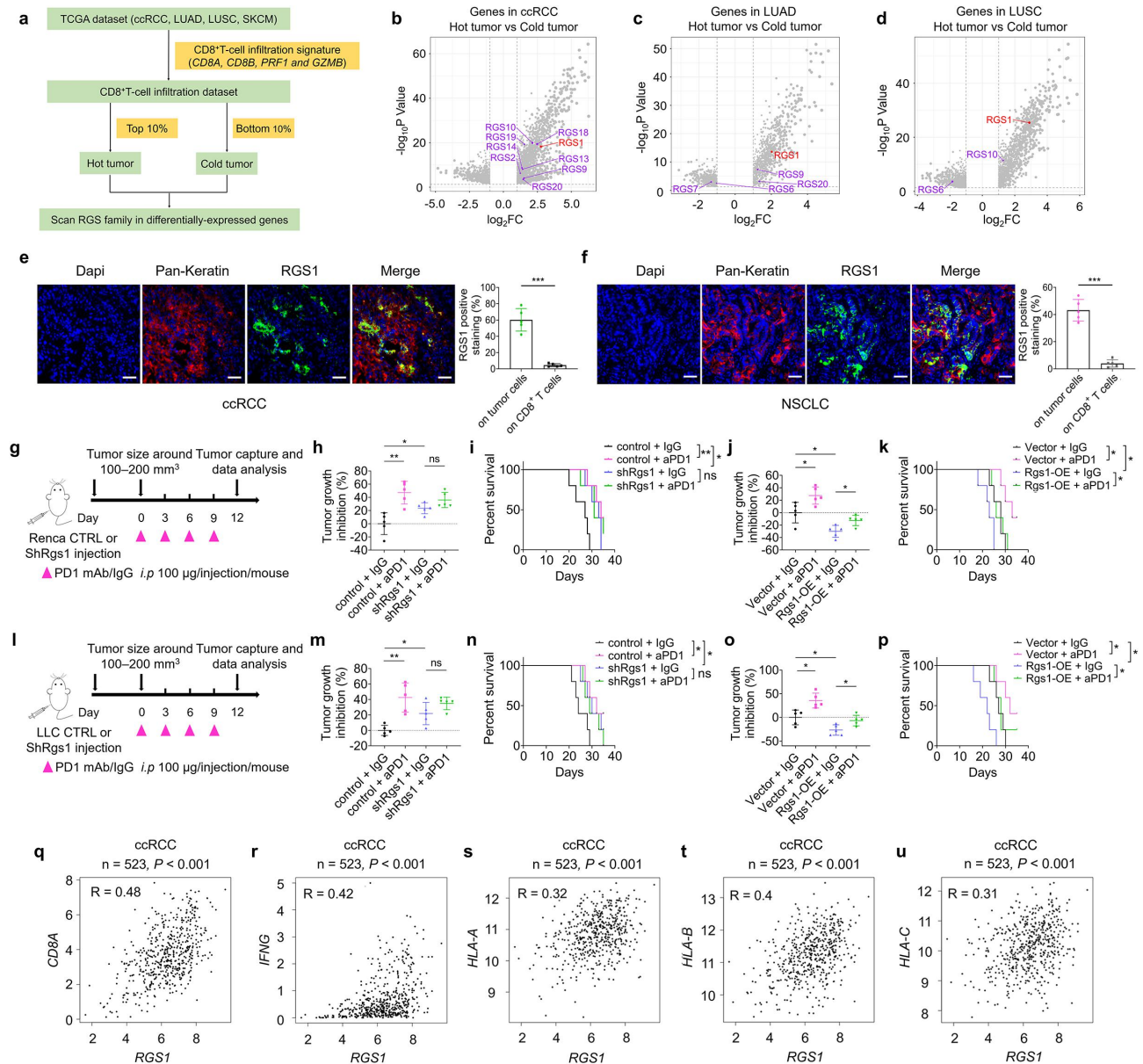


Figure 1. RGS1 in neoplastic cells is positively associated with tumor immunogenicity. **a** The flow chart of RGS1 was screened out. **b–d** Human ccRCC samples (TCGA dataset, KIRC, $n = 523$ patients) and NSCLC samples (TCGA dataset, LUAD, $n = 483$ patients, LUSC, $n = 486$ patients) were divided into “hot” and “cold” tumors on the basis of CD8⁺ T cell infiltration (CD8A, CD8B, PRF1, and GZMB). The volcano plots show the fold changes and p values of RGS family candidates in “hot” tumors (CD8⁺ T cell infiltration, top 10%) versus “cold” tumors (CD8⁺ T cell infiltration, bottom 10%). Statistical analysis was performed using two-sided t -tests. **e, f** Immunofluorescence staining of RGS1 localization on tumor cells in representative samples of human ccRCC (**e**) and NSCLC (**f**). Right, quantification of RGS1 positive staining on tumor cells and CD8⁺ T cells. scale bar, 50 μ m. **g–k** Balb/c mice were subcutaneously (*s.c.*) implanted with 2×10^5 ShRgs1/CTRL (**g–i**) or Rgs1-OE/Vector (**j, k**) Renca cells. When tumor volumes reached 100–200 mm³, mice were intraperitoneally (*i.p.*) administered with PD1 mAb or IgG. **g** A schematic view of the treatment plan. **h** Summary of end-point tumor growth inhibition data. **i** Kaplan–Meier survival curves for each group. **j** Summary of end-point tumor growth inhibition data. **k** Kaplan–Meier survival curves for each group. **l–p** C57BL/6 mice were subcutaneously (*s.c.*) implanted with 2×10^6 ShRgs1/CTRL (**l–n**) or Rgs1-OE/Vector (**o, p**) LLC cells. When tumor volumes reached 100–200 mm³, mice were intraperitoneally (*i.p.*) administered with PD1 mAb or IgG. **l** A schematic view of the treatment plan. **m** Summary of end-point tumor growth inhibition data. **n** Kaplan–Meier survival curves for each group. **o** Summary of end-point tumor growth inhibition data. **p** Kaplan–Meier survival curves for each group. **q–u** Correlation of RGS1 with CD8A (**q**), IFNG (**r**), HLA-A (**s**), HLA-B (**t**) and HLA-C (**u**) in patients with ccRCC (TCGA, KIRC). ns., not significant; * $p < .05$, ** $p < .01$, *** $p < .001$.

samples), NSCLC (LUAD, 483 samples and LUSC, 486 samples) and melanoma (SKCM, 461 samples) cohorts from The Cancer Genome Atlas (TCGA) by dividing tumors into “hot” and “cold” types based on CD8⁺ T cell infiltration (*CD8A*, *CD8B*, *PRF1*, and *GZMB*) and identified 2669, 1366, 1914, and 2209 genes in KIRC, LUAD, LUSC, and SKCM cohorts, respectively, that expressed differentially between “hot” and “cold” tumors ($|\log_2FC| > 1$, $p < .05$). *IFNG*, *CD69*, and *PDL1* were upregulated in “hot” tumors (Table S4), which indicated enhanced CD8⁺ T cell activation. By screening RGS family in the differentially expressed genes, we found they substantially enriched in “hot” tumors. Among the enriched RGS family genes, fold change of *RGS1* ranked top in ccRCC, NSCLC, and second top in melanoma (Figure 1b–d, Supplementary Fig. s2e); detailed fold changes and *p* values for RGS family in these malignancies were shown in Table S5–S8.

By analysis on TCGA database, we found the enrichment of *RGS1* in “hot” tumors. However, although “hot” tumors are infiltrated with abundant CD8⁺ T cells, those CD8⁺ T cells with high expression of *RGS1* are difficult to recruit to or survive in the tumor microenvironment;^{16,21} thus, other cell components should be responsible for the higher expression of *RGS1* in “hot” tumors. Considering the dominant component within a tumor, we suggested rational investigation on the expression and potential function of *RGS1* in neoplastic cells. Above all, we performed immunofluorescence staining on tumor sections obtained from ccRCC and NSCLC patients. As shown in Figure 1e–f, we found that *RGS1* was abundantly distributed in neoplastic cells of ccRCC and NSCLC by observation of dual signals of pan-keratin and *RGS1* within tumors. However, in adjacent slides, the proportion of *RGS1* expression in CD8⁺ T cells was significantly lower than that in tumor cells (Figure 1e–f, Supplementary Fig. s1a–b).

Given the elevated expression of *RGS1* in “hot” tumors, we subsequently utilized two “hot” tumor models to determine the role of *RGS1* in checkpoint therapy. Mice were subcutaneously inoculated with Renca and LLC stably expressing ShRgs1/CTRL or Rgs1-OE/Vector (Supplementary Fig. s1c–f), and were administered with monoclonal anti-PD1 or IgG every 3 d (Figure 1g, l). As shown in Figure 1h–i, compared to CTRL group, *RGS1* knockdown slightly retarded Renca tumor growth with an inhibition rate of 23.4 ($p = .022$), and prolonged mice survival. However, we surprisingly found that although anti-PD1 treatment exhibited approximately 47.1% ($p = .0022$) growth inhibition of CTRL tumors, it failed to protect tumor-bearing mice in *RGS1* knockdown group. Conversely, overexpression of *RGS1* substantially aggravated tumor growth and impaired the survival outcomes, whereas significantly enhanced the efficacy of PD1 inhibition, consistently (Figure 1j–k). Analogical results to that of the murine model of NSCLC were observed (Figure 1m–p). These data suggest that *RGS1* in neoplastic cells benefits anti-PD1 therapy and *RGS1* inhibition elicited immunotherapy resistance.

To further determine the correlation between *RGS1* and immunogenicity, we performed bioinformatics analysis and found the level of *RGS1* positively correlated with the levels of *CD8A*, *IFNG* and *MHCI* (*HLA-A*, *HLA-B*, *HLA-C*), respectively, in the KIRC dataset (Figure 1q–u). Similar correlations were also revealed in NSCLC and melanoma (Supplementary Fig. s2i–m,

Fig. s3h–l). In line with this, gene-set enrichment analysis (GSEA) revealed that *RGS1* expression was associated with JAK-STAT signaling pathway, antigen processing and presentation, immune response and immune activation (Supplementary Fig. s2a–d, Fig. s2f–h, Fig. s3a–g). Based on these findings, we identified a positive association between tumor-intrinsic *RGS1* and tumor immunogenicity in multiple malignancies.

RGS1 is a modulator of IFN γ -JAK-STAT1 signaling

To uncover the role of *RGS1* in cancer immunogenicity, we further analyzed the gene sets altered by *RGS1* expression by using GSEA in TCGA database. Upon scanning the enriched pathways across these three malignancies, we found IFN γ signaling pathway ranked second top in ccRCC, and highly enriched in NSCLC and melanoma positively associated with *RGS1* augmentation (Figure 2a–d).

IFN γ binds to IFNGR1 and induces phosphorylation of STAT1 (p-STAT1) at Y701, leading to further activation of JAK-STAT1 signaling and regulation of anti-tumor immunity.¹¹ Besides, IFN γ augments the expression of MHC1, thereby elicits immunorecognition and antigen presentation.²² To uncover the role of *RGS1* in IFN γ signaling, we stably knocked down *RGS1* with small hairpin RNAs (shRGS1) in RCC cell line 786O (human) and Renca (mouse) and stimulated them with recombinant IFN γ for 2 hours. Following IFN γ stimulation, a remarkable increase in STAT1 phosphorylation (Y701) was observed; whereas, such phosphorylation could be reversed by *RGS1* knockdown (Figure 2e, g), and similar results to that of NSCLC cell line A549 (human) and LLC (mouse) were observed (Supplementary Fig. S4a, c). In addition, we stably overexpressed *RGS1* in the above cell lines and showed that overexpression of *RGS1* significantly enhanced the activation of STAT1 (Figure 2i, k; Supplementary Fig. s4e, g). Along with STAT1 pathway, the expression of PD-L1 was reduced by *RGS1* inhibition (Supplementary Fig. s5a–d), and augmented by *RGS1* overexpression (Supplementary Fig. s6a–d). Meanwhile, we examined the mRNA levels of IFN γ -inducible genes including *STAT1*, *IRF1*, and *IRF9* during IFN γ stimulation and *RGS1* knockdown. In 786O and Renca cells, *RGS1* knockdown notably attenuated IFN γ -induced augmentations of these genes (Figure 2f, h), and the alterations of their protein levels were confirmed (Figure 2e, g); further, the above experiments were also repeated with A549 and LLC cells (Supplementary Fig. s4b, d). Consistent with these data, ectopic *RGS1* expression substantially increased both mRNA transcript and protein levels of *STAT1*, *IRF1*, and *IRF9* upon stimulation with IFN γ (Figure 2j, l; Supplementary Fig. s4f, h).

CXCL9 is another IFN γ -inducible gene. The activation of IFN γ -STAT1 pathway regulates CTL trafficking via increasing CXCL9 transcription.²³ By using an ELISA kit, we also examined the secretion of CXCL9 in Renca and LLC upon *RGS1* knockdown, which turned out a consistent trend (Figure 2m, n). In addition, considering that IFNGR1 is a key regulator lying upstream in the IFN γ

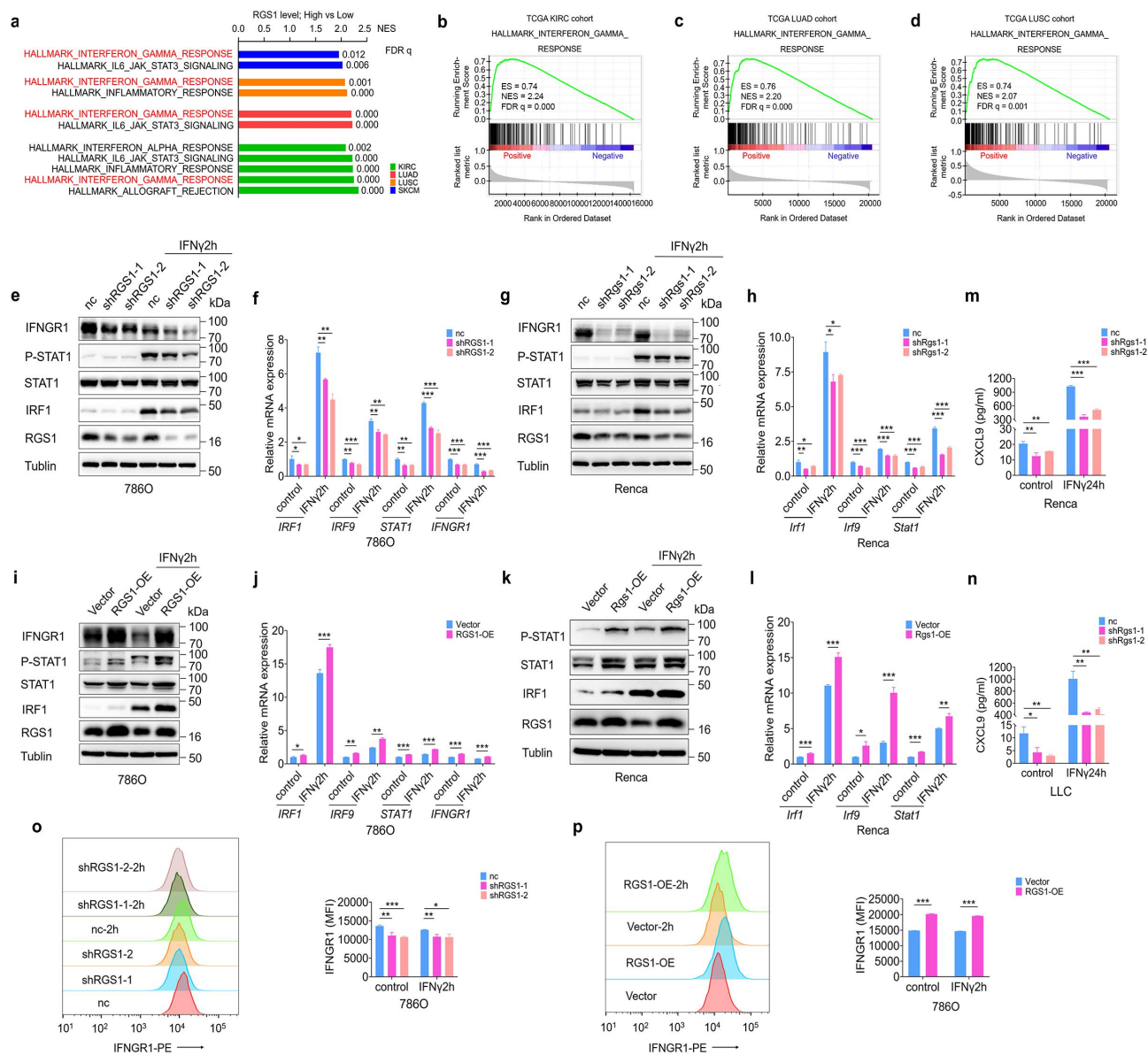


Figure 2. RGS1 is a modulator of IFN γ -JAK-STAT1 signaling. **a** Differentially expressed cancer-related gene sets (H_Hallmarks) with high *RGS1* expression in the KIRC cohort, LUAD cohort, LUSC cohort, and SKCM cohort from TCGA. NES, normalized enrichment score. FDR q, false discovery rate q value. **b** – **d** GSEA output of genes in the HALLMARK_INTERFERON_GAMMA_RESPONSE by *RGS1* high and low expression groups from the KIRC cohort (**b**), LUAD cohort (**c**) and LUSC cohort (**d**) in the TCGA database. ES, enrichment score. **e** – **l** Analysis of IFN γ -STAT1 signaling in 786O and Renca cells. Cell lysates of 786O and Renca cells stably expressing nc or shRGS1 (**e**, **g**) and Vector or RGS1-OE (**i**, **k**) were analyzed by western blotting using RGS1, STAT1, P-STAT1 (Y701), IFNGR1, and IRF1 antibodies. Tubulin was used as an internal control. **f**, **j** IFN γ -inducible gene expression in 786O cells. mRNA expression of *IRF1*, *IRF9*, *STAT1*, and *IFNGR1* were detected by real-time qPCR. Actin was used as an internal control. **h**, **l** IFN γ -inducible gene expression in Renca cells. mRNA expression of *Irf1*, *Irf9*, and *Stat1* were detected by real-time qPCR. Actin was used as an internal control. Cells in **e**, **f**, **i**, **j** were stimulated with 10 ng/ml human recombinant IFN γ or 0.1% BSA negative control for 2 h. Cells in **g**, **h**, **k**, **l** were stimulated with 5 ng/ml mouse recombinant IFN γ or 0.1% BSA negative control for 2 h. **m**, **n** IFN γ -induced CXCL9 secretion. Renca (**m**) and LLC (**n**) cells were cultured in serum-free medium and treated with 5 ng/ml IFN γ for 24 h. The concentration of CXCL9 was analyzed using an ELISA kit. **o**, **p** Cell surface levels of IFNGR1 in nc or shRGS1 (**o**) and Vector or RGS1-OE (**p**) 786O cells (pre-gated with FSC-A vs. SSC-A, and FSC-A vs. FSC-H). Cells were treated with 10 ng/ml IFN γ for 2 h. Right, quantification of the mean fluorescence intensity (MFI). Unpaired t-test was performed with GraphPad Prism 9. All data are representative of three independent experiments. Data in the bar graphs represent mean \pm S.D., $n = 3$. * $p < .05$, ** $p < .01$, *** $p < .001$.

signaling, we further evaluated the expression levels of *IFNGR1* in 786O or A549 cells and demonstrated that RGS1 knockdown reduced *IFNGR1* regardless of IFN γ treatment, either at mRNA (Figure 2f, Supplementary Fig. s4b) or protein levels (Figure 2e, Supplementary Fig. s4a). Conversely, RGS1 overexpression led to elevation of *IFNGR1* (Figure 2i, j, Supplementary Fig. s4e, f). Moreover, we confirmed that silencing or overexpression of RGS1 exerted compatible regulative roles on surface

IFNGR1 expression by using flow cytometry (Figure 2o, p, Supplementary Fig. s4i, j). Taken together, these data suggest that RGS1 serves as a modulator of IFN γ -STAT1 signaling pathway and IFNGR1 expression.

RGS1 regulates antigen presentation via MHC1 pathway

Given the potential connection between RGS1 and antigen presentation and processing pathway revealed by GSEA analysis

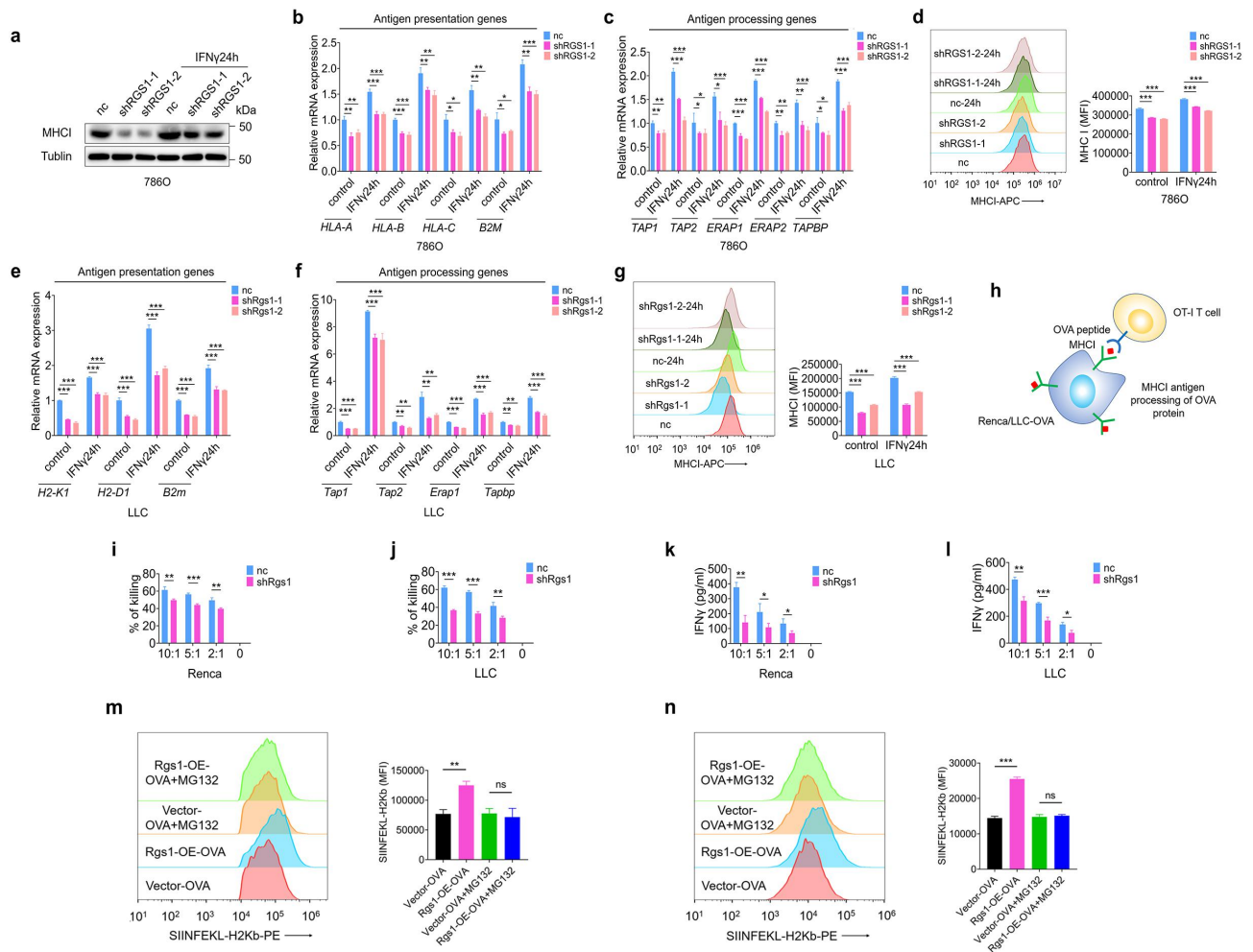


Figure 3. RGS1 regulates antigen presentation via MHC1 pathway. **a** Western blotting of MHC1 in 786O cells stably expressing nc or shRGS1. **b**, **c** mRNA expression of antigen presentation (**b**) and antigen processing genes (**c**) in nc and shRGS1 786O cells. **d** Cell surface levels of MHC1 in nc and shRGS1 786O cells. Right, quantification of the MFI. Cells in **a** – **d** were stimulated with 10 ng/ml human recombinant IFN γ or 0.1% BSA negative control for 24 h. **e**, **f** mRNA expression of antigen presentation (**e**) and antigen processing genes (**f**) in nc and shRgs1 LLC cells. **g** Cell surface levels of MHC1 in nc and shRgs1 LLC cells. Right, quantification of the MFI. Cells in **e** – **g** were stimulated with 10 ng/ml mouse recombinant IFN γ or 0.1% BSA negative control for 24 h. **h** Schematic showing co-culture assay of Renca/LLC-OVA and OT-I T cells. Stable expression of full-length OVA in Renca/LLC cells can evaluate the function of the intracellular MHC1 antigen presentation and processing pathway. Processed OVA peptide bound to MHC1 is presented at the tumor cell surface and recognized by co-cultured antigen-specific OT-I T cells. **i**, **j** Killing effect of nc or shRgs1 Renca-OVA (**i**) and LLC-OVA (**j**) cells after coculture with OT-I T cells. **k**, **l** The production of IFN γ of OT-I T cells cocultured with Renca (**k**) and LLC (**l**) cells were determined by ELISA. **m**, **n** Cell surface levels of SIINFEKL presented by H2Kb in Rgs1-OE-OVA Renca (**m**) and LLC (**n**) cells. Cells were treated with 10 μ M MG132 for 12 h. Right, quantification of the mean fluorescence intensity (MFI). Data in the bar graphs represent mean \pm S.D., $n = 3$. * $p < .05$, ** $p < .01$, *** $p < .001$.

across three tumor types, we evaluated whether RGS1 in neoplastic cells could influence MHC1 expression and the subsequent antigen presentation. As MHC1 is an IFN γ -responsive gene, 24-hour stimulation of IFN γ increased both levels of antigen presenting genes (*HLA-A*, *HLA-B*, *HLA-C* and *B2M*) and antigen processing genes (*ERAP1/2*, *TAP1/2*, and *TAPBP*) in 786O (Figure 3a–c) and A549 cells (Supplementary Fig. s7a – c), as well as murine cell lines (Figure 3e–f, Supplementary Fig. s7e – f), which can be reversed by RGS1 silencing. Similarly, RGS1 knockdown decreased cell-surface MHC1 (Figure 3d, g, Supplementary Fig. s7d, g) whereas overexpression of RGS1 upregulated antigen presentation and processing genes and restored expression of cell surface MHC1 (Supplementary Fig. s8a – h, Fig. s9a – f).

To determine whether RGS1 silencing inhibited antigen processing and presentation and suppressed CTL response,

we engineered Renca and LLC to express full-length foreign protein chicken ovalbumin (OVA). OVA was processed intracellularly to produce SIINFEKL peptide, which was loaded onto MHC1 (H-2Kb) and specifically recognized by the OT-I T-cell receptor (Figure 3h). TCR-transgenic OT-I CD8⁺ T cells were isolated from mice spleens using magnetic beads (Supplementary Fig. s10), and cocultured with OVA-positive Renca/LLC cells transiently transfected with nc and shRgs1. In line with expectations, we found that compared with nc cells, shRgs1 cells showed diminished IFN γ production and aggravated resistance to the cytotoxicity of OT-I CD8⁺ T cells (Figure 3i–l). Further, by overexpressing OVA on Rgs1-OE cells, we observed an increase in SIINFEKL presented by H2Kb on the cell surface (Figure 3m, n). In addition, inclusion of MG132, an inhibitor of antigen processing machinery, prevented the upregulation of the surface presentation of

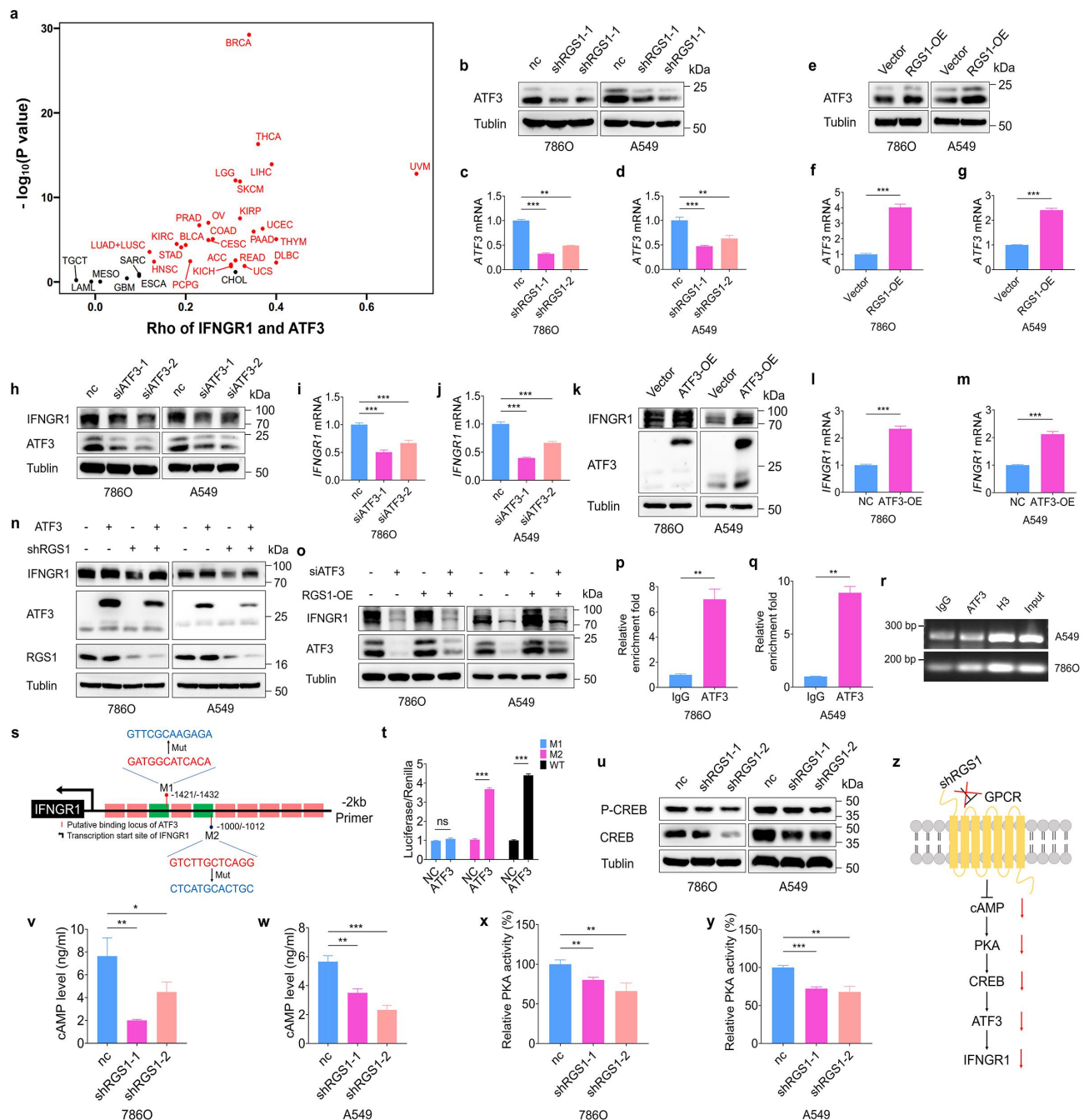


Figure 4. RGS1 promotes ATF3 binding to IFNGR1 promoter. a Spearman correlation analysis of *IFNGR1* and *ATF3* from TCGA database. The red dots indicate p values $< .05$. b Western blotting of ATF3 in 786O and A549 cells stably expressing nc or shRGS1. c, d mRNA expression of *ATF3* in 786O (c) and A549 (d) cells stably expressing nc or shRGS1. e Western blotting of ATF3 in 786O and A549 cells stably overexpressing vector or RGS1. f, g mRNA expression of *ATF3* in 786O (f) and A549 (g) cells stably overexpressing vector or RGS1. h Western blotting of IFNGR1 in 786O and A549 cells transfected with nc or siATF3. i, j mRNA expression of *IFNGR1* in 786O (i) and A549 (j) cells transfected with nc or siATF3. k Western blotting of IFNGR1 in 786O and A549 cells transfected with vector or ATF3-overexpressing plasmid. l, m mRNA expression of *IFNGR1* in 786O (l) and A549 (m) cells transfected with vector or ATF3-overexpressing plasmid. n Western blotting of IFNGR1, ATF3, and RGS1 in 786O and A549 cells stably expressing nc or shRGS1 after transfection with vector or ATF3-overexpressing plasmid. o Western blotting of IFNGR1 and ATF3 in 786O and A549 cells stably overexpressing vector or RGS1 after transfection with nc or siATF3. p – r ChIP-qPCR assay of ATF3, normal IgG and positive control Histone 3 in 786O (p) and A549 (q) cells. s putative ATF3-binding sites in *IFNGR1* promoter with two mutant sites marked as red vertical lines. t Luciferase assay of corresponding mutant sites on the activity of pmirGLO-*IFNGR1* reporter in 293T cells. u Western blotting of CREB and p-CREB in 786O and A549 cells stably expressing nc or shRGS1. v, w Measurement of cAMP level in 786O (v) and A549 (w) cells stably expressing nc or shRGS1 by ELISA. x, y Measurement of PKA activity in 786O (x) and A549 (y) cells stably expressing nc or shRGS1 by ELISA. z Schematic diagram of RGS1 downstream signaling pathway. ns., not significant; * $p < .05$, ** $p < .01$, *** $p < .001$.

SIINFEKL on H2Kb induced by RGS1 overexpression (Figure 3m, n). Together, these data suggest that RGS1 silencing could suppress CD8⁺ T-cell-mediated anti-tumor response through reduction of MHC1 expression.

RGS1 promotes ATF3 binding to IFNGR1 promoter

It has been well established that RGS1 negatively regulates intracellular signaling of GPCRs by RGS domain that activates GTPase and suppresses G protein.²⁴ As a GPCR, the adenosine

A1 receptor (ADORA1) has been recently reported to be involved in tumor immune escape inhibition through regulating ATF3 and PD-L1.¹⁹ ATF3 functions as a transcription factor that can be induced by various cellular stresses.²⁵ Accordingly, we wondered whether ATF3 is responsible for the mechanism by which RGS1 regulates IFNGR1. By analysis of TCGA database, the expression level of *ATF3* displayed positive correlation with *IFNGR1* among a variety of cancer types (Figure 4a). We further validated the association of RGS1 and ATF3 in 786O and A549 cells, and found that RGS1 knockdown led to a remarkable reduction of ATF3 both at protein (Figure 4b) and mRNA levels (Figure 4c, d), which is consistent with the data that stable overexpression of RGS1 enhanced the level of ATF3 (Figure 4e–g). Moreover, ATF3 silenced by transient transfection of specific siRNAs notably decreased mRNA (Figure 4i, j) and protein levels (Figure 4h) of *IFNGR1*, and overexpression of ATF3 augmented the level of *IFNGR1*, conversely (Figure 4k–m). Further, the expression of IFNGR1 in 786O and A549 cells inhibited by RGS1 silencing could be rescued by overexpression of ATF3 (Figure 4n), and IFNGR1 augmented by RGS1 overexpression could also be rescued by knockdown of ATF3 (Figure 4o). Thus, these data indicate that ATF3 serves as an essential modulator for RGS1 to provoke IFNGR1 expression.

To determine whether ATF3, as a transcription factor, direct targets *IFNGR1*, we identified two putative-binding sites for ATF3 at –1421/–1432 and –1000/–1012 in the promoter region of human *IFNGR1* via JASPAR (<http://jaspar.genereg.net/>). By means of CHIP-qPCR assay, we showed that more chromatin of *IFNGR1* were precipitated with anti-ATF3 than with IgG in 786O and A549 cells (Figure 4p–r), which confirmed that ATF3 could directly bind to *IFNGR1* promoter, thereby regulating transcription of *IFNGR1*. Further, we constructed promoter fragments containing mutations in the two identified regions to prevent ATF3 from binding properly (Figure 4s). To determine whether the two putative ATF3 binding regions were transcriptional active, we performed a dual luciferase assay in 293T and revealed that mutation of *IFNGR1* promoter at –1421/–1432 site led to a significantly decreased luciferase activity in Flag-ATF3 overexpressing group compared with control group, while that of the other site showed negligible change (Figure 4t). Collectively, we demonstrated that ATF3 regulated IFNGR1 expression through directly binding to the site (–1421/–1432) in the *IFNGR1* promoter region in NSCLC and ccRCC.

In addition, we evaluated whether RGS1 regulates ATF3 via the cAMP/protein kinase A (PKA)/cAMP-response element binding protein (CREB) axis as reported.¹⁹ Our results revealed a decreased cAMP level and PKA activity induced by RGS1 knockdown in 786O and A549 cells (Figure 4v–y). Additionally, silencing of RGS1 also distinctly impaired the activity of CREB (Figure 4u). Further, we included 666–15, an inhibitor of CREB pathway (Supplementary Fig. s11a, b), and demonstrated that the expression of ATF3 was no longer changed by RGS1 knockdown when 666–15 was added

(Supplementary Fig. s11c, d). In line with our findings, ATF3 can directly bind to the promoter region of *STAT1* to improve its transcription and activates IFN γ signaling.²⁶ Together, these data suggest that RGS1 augments IFNGR1 expression through RGS1/cAMP/PKA/CREB/ATF3/IFNGR1 axis (Figure 4z).

RGS1 is associated with T cell infiltration in RCC and NSCLC mouse models

Given the regulative mechanism of RGS1 on IFN γ -STAT1 signaling in vitro, we further evaluated its role in ATF3/IFNGR1 axis and T cell infiltration in RCC and NSCLC murine models. By IHC analysis, we found that expression levels of ATF3 and IFNGR1 were decreased in Renca and LLC tumors stably expressing ShRgs1, compared with CTRL group (Figure 5a). Similarly, a remarkably diminished level of CXCL9 was also observed in the ShRgs1 tumors (Figure 5a). Substantially, we evaluated T cell infiltration within the tumor mass. Figure 5b reveals decreased infiltration of CD3⁺ T cells, CD4⁺ T cells, CD8⁺ T cells and repressed PD1 expression within ShRgs1 tumors. Through validating by immunofluorescence staining, we observed less CD8⁺ T cells accompanied with PD1 expression in ShRgs1 tumors, indicating that fewer exhausted TILs could be unleashed by PD1 inhibition in tumors lack of RGS1 (Figure 5c). Similar results were observed in a murine model of NSCLC (Figure 5d–f). Conversely, overexpression of RGS1 in tumor cells was associated with increased accumulation of CD3⁺ T cells, CD4⁺ T cells, and CD8⁺PD1⁺ T cells as expected (Supplementary Fig. s12a – d). These data collectively suggest that RGS1 in neoplastic cells regulates ATF3/IFNGR1 axis and T cell infiltration probably via secretion of CXCL9 in RCC and NSCLC murine models.

RGS1-ATF3-IFNGR1 axis is associated with the efficacy of PD1 inhibition therapy in clinical samples

To strengthen our findings in human cancer patient samples, we analyzed a link between RGS1, ATF3 and IFNGR1 in a cohort of 41 patients with ccRCC. IHC analysis showed that RGS1 was positively associated with ATF3 and IFNGR1 in tumor tissues, respectively (Supplementary Fig. s13a – d). Further, we validated our findings in a cohort of 21 NSCLC patients receiving monoclonal anti-PD1 therapy by dividing these patients into 10 responders and 11 not-responders, based on their responses. By means of multiple immunofluorescence staining, we observed elevated RGS1, ATF3, and IFNGR1 expression in the tumors of responders, accompanied with enhanced infiltration of CD8⁺PD1⁺ T cells (Figure 6a–e). These findings were consistent with our previous in vivo and in vitro results, indicating that RGS1 displayed positively correlation with ATF3, IFNGR1, and tumor response to immunotherapy.

In line with the pathological findings above, radiological examination also demonstrated such association. Figure 6g shows two representative cases with pathological graphs before and after immunotherapy treatment where the radiologist indicated the diameter of the NSCLC tumor with red arrows. Based on the immunofluorescence analysis of RGS1 expression, we divided NSCLC puncture biopsy specimens into

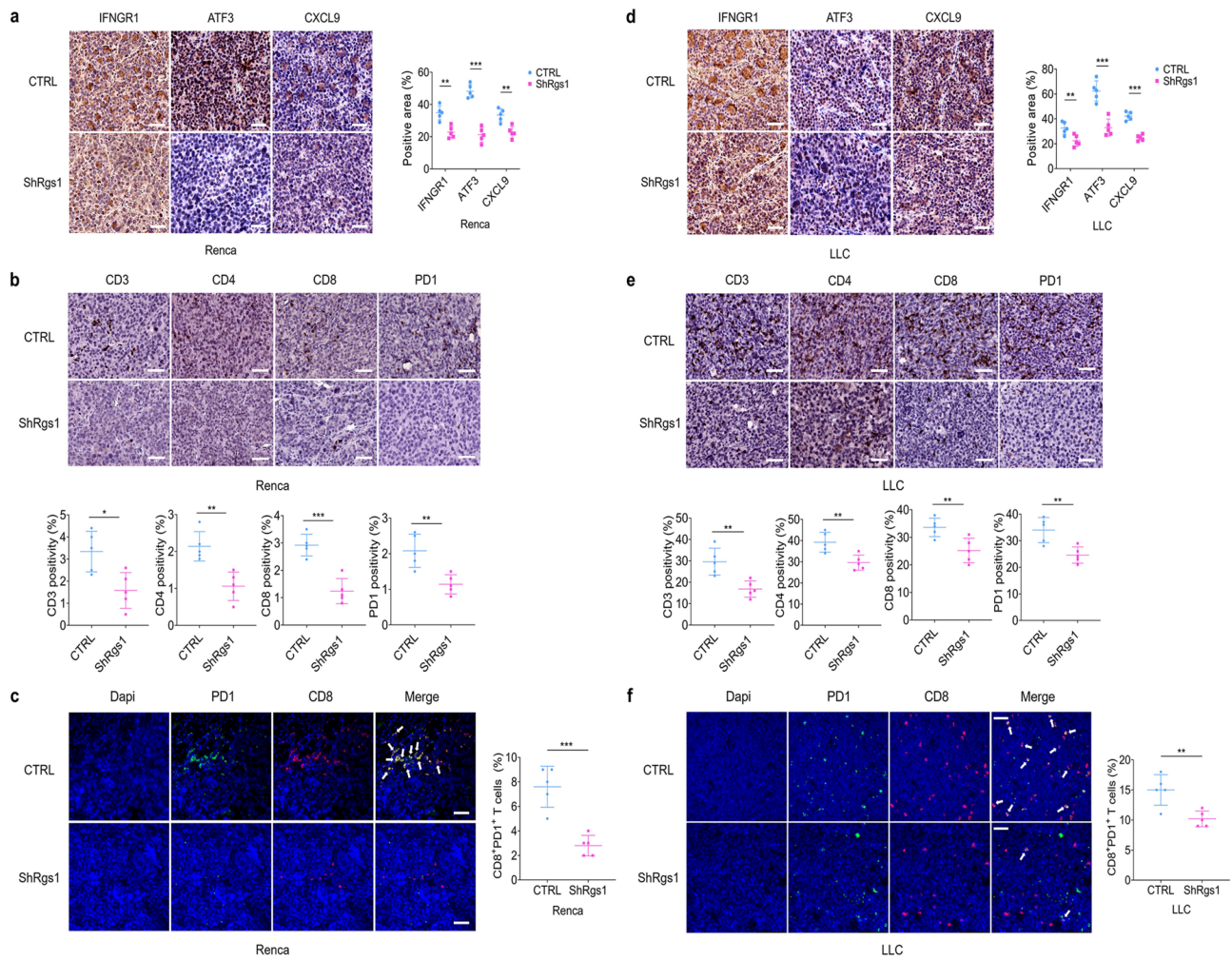


Figure 5. RGS1 is associated with T cell infiltration in RCC and NSCLC mouse models. **a, d** Representative images and quantification (right) of immunohistochemistry staining of IFNGR1, ATF3 and CXCL9 expression in harvested CTRL and ShRgs1 Renca (**a**) or LLC (**d**) subcutaneous tumor sections. The percentages of positively stained area (right) were analyzed using Image J software. Scale bar, 100 μ m. **b, e** T cell infiltration and quantification (below) of Renca (**b**) or LLC (**e**) subcutaneous tumor. Paraffin-embedded tissue sections of murine tumors were immunohistochemically stained with antibodies against CD3, CD4, CD8 and PD1. The percentages of positively stained cells (below) were analyzed using Image J software. Scale bar, 100 μ m. **c, f** Representative immunofluorescence images of CD8 and PD1 staining in ShRgs1 or CTRL Renca (**c**) or LLC (**f**) tumor sections. White arrows indicate merge of CD8 and PD1 fluorescence signals. Scale bar, 50 μ m. Data in the graphs represent mean \pm S.D, $n = 5$. * $p < .05$, ** $p < .01$, *** $p < .001$.

relatively high and low groups. Intriguingly, patient 1 with relatively high expression of RGS1 before immunotherapy, showed remarkably reduced lesion diameter after receiving immunotherapy; nevertheless, patient 11 who exhibited low RGS1 level showed tumor enlargement. Further, we analyzed the relationship between tumor lesion diameter changes after immunotherapy and RGS1 expression status before immunotherapy in the 21 NSCLC patients enrolled in this study. Of the 10 patients with high RGS1 expression, 7 had reduced tumor lesions and 3 had enlarged tumor lesions; as a contrast, in the remaining 11 patients with low RGS1 expression, 8 patients suffered from increased tumor size and 3 patients displayed tumor shrinkage (Figure 6f). As such, the correlation coefficient between RGS1 expression status before treatments and tumor diameter changes after immunotherapy was 0.724 ($p < .001$) (Figure 6h). Moreover, clinical association research with these NSCLC patients revealed significant associations between prolonged progression-free survival (PFS) and high

expression levels of RGS1, ATF3, and IFNGR1, respectively (Figure 6i–k), which is consistent with the previous report that ATF3 positively correlated with response to PD1 inhibition therapy in NSCLC.¹⁹ Taken together, these data indicate that RGS1 can be utilized as a promising predictor for the response to anti-PD1 immunotherapy, which potentially gives impetus to personalized ICB therapy at least in NSCLC.

Discussion

In the present study, we identified tumor-intrinsic RGS1 as positively associating with immunogenicity through bioinformatics analysis of TCGA data across several malignancies, and investigated the impact of RGS1 on IFN γ -STAT1 signaling and antigen presentation in cancer cells. By further employing murine allograft tumor models and human NSCLC datasets, we validated the role of RGS1 on response to immunotherapy. Overall, these findings suggest that tumor-intrinsic RGS1

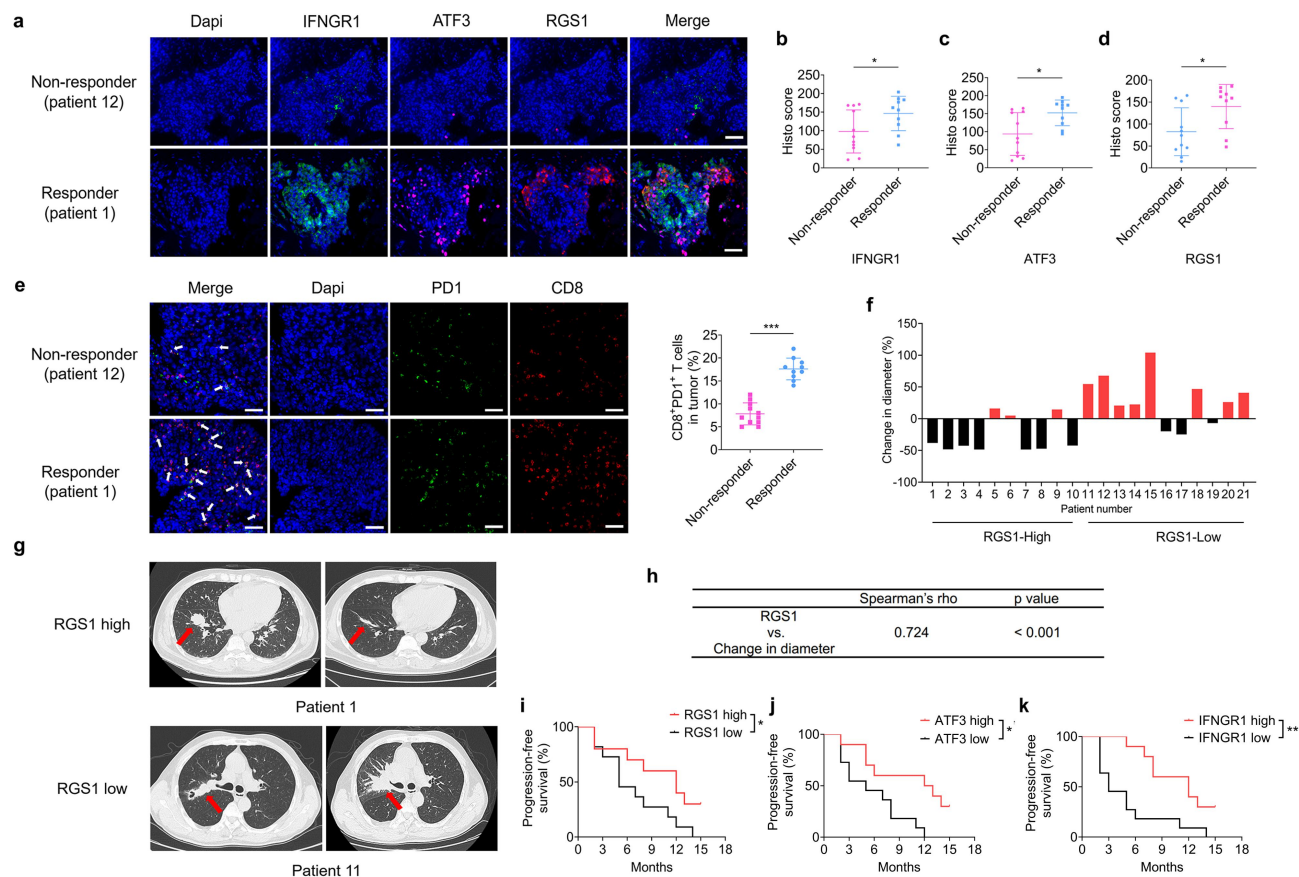


Figure 6. RGS1-ATF3-IFNGR1 axis is associated with the efficacy of PD1 inhibition therapy in clinical samples. a – d Representative images (a) and quantification of immunofluorescence staining for IFNGR1(b), ATF3(c) and RGS1 (d) expression in NSCLC responder ($n = 10$) and non-responder ($n = 11$) specimens. Scale bar, 50 μ m. e Representative immunofluorescence images of CD8 and PD1 staining in NSCLC responder and non-responder specimens. White arrows indicate merge of CD8 and PD1 fluorescence signals. Right, quantification of CD8⁺PD1⁺ T cells in tumor. Scale bar, 50 μ m. f Change in tumor diameter for all NSCLC patients ($n = 21$), where those with increased tumor diameter are shown in red. g Representative radiological images for NSCLC responder and non-responder cases receiving PD1 inhibition treatment. Tumor diameter based on the CT imaging was annotated by the radiologist with a red line. h Quantitative correlation between tumor diameter changes after anti-PD1 treatment and RGS1 expression levels before that. Correlation coefficients and p values were calculated according to Spearman's rank correlation method. i – k Kaplan–Meier survival curves of NSCLC patients' progression-free survival on basis of the expression level of RGS1 (i), ATF3 (j) and IFNGR1 (k). * $p < .05$, ** $p < .01$, *** $p < .001$.

represents a pivotal modulator in tumor immunotherapeutic response (Supplementary Fig. s14).

CTL-expressed RGS1 and RGS16 have been previously documented to negatively correlate with anti-tumor immune response.^{16,21} Of note, Huang et al. have uncovered an intriguing phenomenon that IFN γ -STAT1 signaling, which lies upstream of RGS1, has distinct effects on tumor cells and circulating CTLs in regard to T cell recruitment. Specifically, in circulating CTLs and T_H1 cells, STAT1 activation impedes T cell migration, while in tumor cells, it retains T cells within the tumor mass and provokes anti-tumor immune response.¹⁶ The opposed functions of RGS1 in neoplastic cells and T cells is consistent with that of IFN γ signaling, which establish a regulatory relationship that limits both adaptive and innate immune response to cancer immunotherapy.²⁷ Here in the present study, we first propose the positive association between tumor-intrinsic RGS1 and immunogenicity in more than one malignancy with detailed molecular understandings; even so, further investigations should be proceeded.

Recently, several studies have highlighted the regulation of IFN γ receptors and their nonnegligible roles in anti-tumor immune response,^{10,11,28} which emphasize the importance of

the integrity of IFN γ signaling in checkpoint therapy. In addition, MHC1 signaling is equally essential in anti-tumor immunity, which can be stimulated by IFN γ -STAT1 signaling or manipulated by other mechanisms to influence therapeutic outcomes.^{14,20} Regardless, our data indicate that RGS1 silencing suppresses both IFN γ and MHC1 signaling via diminishing expression of *IFNGR1* and *MHCI* genes transcriptionally, which shifts renal and lung tumors to a “cold” type.

As illustrated by our clinical cases, high expression level of RGS1, which indicates provoked immune response to checkpoint therapy, was accompanied with improved infiltration of CD8⁺PD1⁺ T cells, suggesting that RGS1 could serve as a promising predictor for the response to anti-PD1 therapy. Even so, this result needs to be further verified in a larger public cohort. *RGS1* enrichment was observed in several malignancies including melanoma,²⁹ ccRCC¹⁷ and NSCLC,³⁰ and correlated with shorter overall survival in melanoma and several other cancers.^{31,32} Consistent with our data from preclinical murine models, *RGS1* is probably identified as a tumorigenic regulator in multiple cancer types. In conjunction with the above-mentioned studies, we speculate that although highly expressed RGS1 in neoplastic

cells induces abundant CD8⁺ T cells accumulation within tumors, it simultaneously triggers persistent antigen stimulation through augmented MHCI signaling which further elicits exhaustion of these recruited CD8⁺ T cells, and eventually turns on tumor-promoting effect. Moreover, other genes which promote tumor growth, such as *PBRM1* and *USP22*, also benefit immunotherapy and adoptive T-cell therapy, respectively.^{11,33} Besides, tumor suppressor ELF5 which remarkably inhibits tumor growth, has poor effects on immunotherapy.³⁴

Collectively, we consider there are several noteworthy points here. First, the unknown switch by which neoplastic cells or immune cells manipulate the expression of RGS1 and to what extent is IFN γ pathway involved requires further investigation. Second, the possibility that tumorigenic regulators such as RGS1 benefit immunotherapy puts forward a new angle for future screening of genes related to immunotherapeutic efficacy. Third, paying close attention to the RGS family in multiple cell types and the status of exhausted T cells either before or during the therapeutic process may benefit personalized ICB therapy.

Taken together, our current study unveils a novel molecular mechanism underlying the modulatory effect of tumor-intrinsic RGS1 in immunotherapeutic response, which changes tumor immunogenicity and the susceptibility of tumor cells to T cell killing by regulating IFN γ -STAT1 signaling pathway and the expression of MHCI, and implicates that RGS1 may serve as a predictive marker and a potential target for clinical T-cell-based combination therapy.

List of abbreviations

RGS1	Regulator of G-protein signaling 1
ATF3	Activating Transcription factor 3
IFNGR1	Interferon Gamma Receptor 1
TILs	Tumor-infiltrating lymphocytes
PD-L1	Programmed death ligand 1
ICB	Immune checkpoint blockade
ccRCC	clear cell Renal Cell Carcinoma
NSCLC	Non-small cell lung cancer
GPCR	G-protein coupled receptor
CTLs	Cytotoxic T lymphocytes
CHIP	Chromatin immunoprecipitation
GSEA	Gene Set Enrichment Analysis
TCGA	The Cancer Genome Atlas

Acknowledgments

We thank Prof. H. Tang (Shandong First Medical University, China) and Prof. J. Li (Nanjing University, China) for the donation of Transgenic OT-I mice and mouse lentiviral vector encoding OVA, respectively. In addition, we also thank Prof. YC. Xu (Zhejiang University, China) for his suggestions on the article.

Disclosure statement

No potential conflict of interest was reported by the author(s).

Funding

This work was supported by grants from the National Natural Science Foundation of China (81972388, 82173160 and 82002681) and the Natural Science Foundation of Jiangsu Province (BK20200123).

Authors' contributions

H.G., B.W., and W.D. devised and coordinated the project. B. W. performed all the experiments with help from B.J. and L.D.; W.D., Q.Z. and Y.W. performed bioinformatics analyses. B.J., W.C., M.D. and W.C. performed experiments with the Renca/LLC tumor models. J.G., Y. F. and Y.D. collected clinical samples and performed IHC and IF analyses. B.J., W.D., and H.G. wrote the manuscript. All authors revised the manuscript.

Consent for publication

Patients in the study were in compliance with informed consent policy and gave permission for publication.

Ethics approval and consent to participate

The study protocol was under the approval of the Institutional Review Board of Nanjing Drum Tower Hospital (approval 2017-147-01). The collection of all tissue samples was in compliance with informed consent policy.

References

- Hodi FS, O'Day SJ, McDermott DF, Weber RW, Sosman JA, Haanen JB, Gonzalez R, Robert C, Schadendorf D, Hassel JC, et al. Improved survival with ipilimumab in patients with metastatic melanoma. *N Engl J Med.* 2010;363(8):711–723. doi:10.1056/NEJMoa1003466.
- Garon EB, Rizvi NA, Hui R, Leighl N, Balmanoukian AS, Eder JP, Patnaik A, Aggarwal C, Gubens M, Horn L, et al. Pembrolizumab for the treatment of non-small-cell lung cancer. *N Engl J Med.* 2015;372(21):2018–2028. doi:10.1056/NEJMoa1501824.
- Motzer RJ, Tannir NM, McDermott DF, Arén Frontera O, Melichar B, Choueiri TK, Plimack ER, Barthélémy P, Porta C, George S, et al. Nivolumab plus Ipilimumab versus Sunitinib in Advanced Renal-Cell Carcinoma. *N Engl J Med.* 2018;378(14):1277–1290. doi:10.1056/NEJMoa1712126.
- Zaretsky JM, Garcia-Diaz A, Shin DS, Escuin-Ordinas H, Hugo W, Hu-Lieskovan S, Torrejon DY, Abril-Rodriguez G, Sandoval S, Barthly L, et al. Mutations associated with acquired resistance to PD-1 blockade in melanoma. *N Engl J Med.* 2016;375(9):819–829. doi:10.1056/NEJMoa1604958.
- Shin DS, Zaretsky JM, Escuin-Ordinas H, Garcia-Diaz A, Hu-Lieskovan S, Kalbasi A, Grasso CS, Hugo W, Sandoval S, Torrejon DY, et al. Primary resistance to PD-1 blockade mediated by JAK1/2 mutations. *Cancer Discov.* 2017;7(2):188–201. doi:10.1158/2159-8290.CD-16-1223.
- Manguso RT, Pope HW, Zimmer MD, Brown FD, Yates KB, Miller BC, Collins NB, Bi K, LaFleur MW, Juneja VR, et al. In vivo CRISPR screening identifies Ptpn2 as a cancer immunotherapy target. *Nature.* 2017;547(7664):413–418. doi:10.1038/nature23270.
- Jia H, Song L, Cong Q, Wang J, Xu H, Chu Y, Li Q, Zhang Y, Zou X, Zhang C, et al. The LIM protein AJUBA promotes colorectal cancer cell survival through suppression of JAK1/STAT1/IFIT2 network. *Oncogene.* 2017;36(19):2655–2666. doi:10.1038/onc.2016.418.
- Nagarsheth N, Peng D, Kryczek I, Wu K, Li W, Zhao E, Zhao L, Wei S, Frankel T, Vatan L, et al. PRC2 epigenetically silences Th1-type chemokines to suppress effector T-Cell trafficking in colon cancer. *Cancer Res.* 2016;76(2):275–282. doi:10.1158/0008-5472.CAN-15-1938.
- Peng D, Kryczek I, Nagarsheth N, Zhao L, Wei S, Wang W, Sun Y, Zhao E, Vatan L, Szeliga W, et al. Epigenetic silencing of TH1-type chemokines shapes tumour immunity and immunotherapy. *Nature.* 2015;527(7577):249–253. doi:10.1038/nature15520.

10. Du W, Hua F, Li X, Zhang J, Li S, Wang W, Zhou J, Wang W, Liao P, Yan Y, et al. Loss of optineurin drives cancer immune evasion via palmitoylation-dependent IFNGR1 lysosomal sorting and degradation. *Cancer Discov.* 2021;11(7):1826–1843. doi:10.1158/2159-8290.CD-20-1571.
11. Liu XD, Kong W, Peterson CB, McGrail DJ, Hoang A, Zhang X, Lam T, Pilie PG, Zhu H, Beckermann KE, et al. PBRM1 loss defines a nonimmunogenic tumor phenotype associated with checkpoint inhibitor resistance in renal carcinoma. *Nat Commun.* 2020;11(1):2135. doi:10.1038/s41467-020-15959-6.
12. Shen JZ, Qiu Z, Wu Q, Finlay D, Garcia G, Sun D, Rantala J, Barshop W, Hope JL, Gimble RC, et al. FBXO44 promotes DNA replication-coupled repetitive element silencing in cancer cells. *Cell.* 2021;184(2):352–369.e23. doi:10.1016/j.cell.2020.11.042.
13. Ren J, Li N, Pei S, Lian Y, Li L, Peng Y, Liu Q, Guo J, Wang X, Han Y, et al. Histone methyltransferase WHSC1 loss dampens MHC-I antigen presentation pathway to impair IFN- γ -stimulated antitumor immunity. *Journal Of Clinical Investigation.* 2022;132(8). doi:10.1172/JCI153167.
14. Liu X, Bao X, Hu M, Chang H, Jiao M, Cheng J, Xie L, Huang Q, Li F, Li C-Y, et al. Inhibition of PCSK9 potentiates immune checkpoint therapy for cancer. *Nature.* 2020;588(7839):693–698. doi:10.1038/s41586-020-2911-7.
15. Watson N, Linder ME, Druey KM, Kehrl JH, Blumer KJ. RGS family members: GTPase-activating proteins for heterotrimeric G-protein α -subunits. *Nature.* 1996;383(6596):172–175. doi:10.1038/383172a0.
16. Huang D, Chen X, Zeng X, Lao L, Li J, Xing Y, Lu Y, Ouyang Q, Chen J, Yang L, et al. Targeting regulator of G protein signaling 1 in tumor-specific T cells enhances their trafficking to breast cancer. *Nat Immunol.* 2021;22(7):865–879. doi:10.1038/s41590-021-00939-9.
17. Bai Y, Hu M, Chen Z, Wei J, Du H. Single-cell transcriptome analysis reveals RGS1 as a New Marker and promoting factor for T-Cell exhaustion in multiple cancers. *Front Immunol.* 2021;12:767070. doi:10.3389/fimmu.2021.767070.
18. Burr ML, Sparbier CE, Chan KL, Chan Y-C, Kersbergen A, Lam EYN, Azidis-Yates E, Vassiliadis D, Bell CC, Gilan O, et al. An evolutionarily conserved function of polycomb silences the MHC class I antigen presentation pathway and enables immune evasion in cancer. *Cancer Cell.* 2019;36(4):385–401.e8. doi:10.1016/j.ccell.2019.08.008.
19. Liu H, Kuang X, Zhang Y, Ye Y, Li J, Liang L, Xie Z, Weng L, Guo J, Li H, et al. ADORA1 inhibition promotes tumor immune evasion by regulating the ATF3-PD-L1 axis. *Cancer Cell.* 2020;37(3):324–339.e8. doi:10.1016/j.ccell.2020.02.006.
20. Li G, Kryczek I, Nam J, Li X, Li S, Li J, Wei S, Grove S, Vatan L, Zhou J, et al. LIMIT is an immunogenic lncRNA in cancer immunity and immunotherapy. *Nat Cell Biol.* 2021;23(5):526–537. doi:10.1038/s41556-021-00672-3.
21. Weisshaar N, Wu J, Ming Y, Madi A, Hotz-Wagenblatt A, Ma S, Mieg A, Hering M, Zettl F, Mohr K, et al. Rgs16 promotes anti-tumor CD8+T cell exhaustion. *Sci Immunol.* 2022;7(71):eabh1873. doi:10.1126/sciimmunol.abh1873.
22. Zhou F. Molecular mechanisms of IFN-gamma to up-regulate MHC class I antigen processing and presentation. *Int Rev Immunol.* 2009;28(3–4):239–260. doi:10.1080/08830180902978120.
23. Wang L, Hui H, Agrawal K, Kang Y, Li N, Tang R, Yuan J, Rana TM. m6A RNA methyltransferases METTL3/14 regulate immune responses to anti-PD-1 therapy. *EMBO J.* 2020;39(20):e104514. doi:10.15252/embj.2020104514.
24. Ross EM, Wilkie TM. Gtpase-activating proteins for heterotrimeric G proteins: regulators of G protein signaling (RGS) and RGS-like proteins. *Annu Rev Biochem.* 2000;69(1):795–827. doi:10.1146/annurev.biochem.69.1.795.
25. De Nardo D, Labzin LI, Kono H, Seki R, Schmidt SV, Beyer M, Xu D, Zimmer S, Lahrman C, Schildberg FA, et al. High-density lipoprotein mediates anti-inflammatory reprogramming of macrophages via the transcriptional regulator ATF3. *Nat Immunol.* 2014;15(2):152–160. doi:10.1038/ni.2784.
26. Kim JY, Song EH, Lee S, Lim JH, Choi JS, Koh I-U, Song J, Kim W-H. The induction of STAT1 gene by activating transcription factor 3 contributes to pancreatic β -cell apoptosis and its dysfunction in streptozotocin-treated mice. *Cell Signal.* 2010;22(11):1669–1680. doi:10.1016/j.cellsig.2010.06.007.
27. Benci JL, Johnson LR, Choa R, Xu Y, Qiu J, Zhou Z, Xu B, Ye D, Nathanson KL, June CH, et al. Opposing functions of interferon Coordinate Adaptive and innate immune responses to cancer immune checkpoint blockade. *Cell.* 2019;178(4):933–948.e14. doi:10.1016/j.cell.2019.07.019.
28. Guo W, Wang Y, Yang M, Wang Z, Wang Y, Chaurasia S, Wu Z, Zhang M, Yadav GS, Rathod S, et al. LincRNA-immunity landscape analysis identifies EPIC1 as a regulator of tumor immune evasion and immunotherapy resistance. *Sci Adv.* 2021;7(7):eabb3555. doi:10.1126/sciadv.abb3555.
29. Sun MY, Wang Y, Zhu J, Lv C, Wu K, Wang X, Xue C. Critical role for non-GAP function of Gas in RGS1-mediated promotion of melanoma progression through AKT and ERK phosphorylation. *Oncol Rep.* 2018;39(6):2673–2680. doi:10.3892/or.2018.6341.
30. Dai J, Gu J, Lu C, Lin J, Stewart D, Chang D, Roth JA, Wu X. Genetic variations in the regulator of G-protein signaling genes are associated with survival in late-stage non-small cell lung cancer. *PloS One.* 2011;6(6):e21120. doi:10.1371/journal.pone.0021120.
31. Hu Y, Zheng M, Wang S, Gao L, Gou R, Liu O, Dong H, Li X, Lin B. Identification of a five-gene signature of the RGS gene family with prognostic value in ovarian cancer. *Genomics.* 2021;113(4):2134–2144. doi:10.1016/j.ygeno.2021.04.012.
32. Roh J, Shin S-J, Lee A-N, Yoon DH, Suh C, Park C-J, Huh J, Park C-S. RGS1 expression is associated with poor prognosis in multiple myeloma. *J Clin Pathol.* 2017;70(3):202–207. doi:10.1136/jclinpath-2016-203713.
33. Li M, Xu Y, Liang J, Lin H, Qi X, Li F, Han P, Gao Y, Yang X. USP22 deficiency in melanoma mediates resistance to T cells through IFN γ -JAK1-STAT1 signal axis. *Mol Ther.* 2021;29(6):2108–2120. doi:10.1016/j.ymthe.2021.02.018.
34. Singh S, Kumar S, Srivastava RK, Nandi A, Thacker G, Murali H, Kim S, Baldeon M, Tobias J, Blanco MA, et al. Loss of ELF5-FBXW7 stabilizes IFNGR1 to promote the growth and metastasis of triple-negative breast cancer through interferon- γ signalling. *Nat Cell Biol.* 2020;22(5):591–602. doi:10.1038/s41556-020-0495-y.